ISBN: 978-3-95450-234-9 ISSN: 2673-5504 doi:10.18429/JACoW-SRF2023-MOPMB005

MUON SPIN ROTATION STUDIES OF BILAYER SUPERCONDUCTORS AND LOW TEMPERATURE BAKED NIOBIUM

Md Asaduzzaman[1,*], Ryan M. L. McFadden[1], Edward Thoeng[2],
Robert E. Laxdal, Tobias Junginger[1,†], TRIUMF, Vancouver, Canada
[1]also at Department of Physics and Astronomy, University of Victoria, Victoria, Canada
[2]also at Department of Physics and Astronomy, University of British Columbia, Vancouver, Canada

Abstract

Muon spin rotation (μSR) results have shown that the first vortex penetration field detected by muons ($H_{\mathrm{vp},\mu}$) into Nb can be delayed up to the superheating field, H_{sh} by coating a single layer of a material with larger London penetration depth, λ_{L}. For low-temperature baked (LTB) (i.e., 120 °C baked) Nb an increase in the $H_{\mathrm{vp},\mu}$ has also been observed. While clearly exceeding the lower critical field H_{c1}, $H_{\mathrm{vp},\mu}$ was found to remain significantly below H_{sh} for LTB Nb. Further, magnetometry experiments suggested that there is no interface barrier in LTB Nb and that the apparent $H_{\mathrm{vp},\mu}$ increase as observed by μSR was due to surface pinning. By varying the implantation depth of muons of $E \sim 4.1$ MeV using moderating foils, new μSR measurements confirm that the apparent $H_{\mathrm{vp},\mu}$ increase in LTB Nb is indeed due to surface pinning, while for a Nb_3Sn (2 µm)/Nb bilayer we find that an interface energy barrier prevents flux penetration. These results confirm the potential of using superconducting bilayers to achieve a flux free Meissner state up to the H_{sh} of the substrate.

BACKGROUND

Superconducting radio frequency (SRF) cavities need to be operated in a flux free Meissner state to avoid strong dissipation from magnetic vortices. The maximum field that can be sustained by a superconductor in the Meissner state is proportional to the accelerating gradient (E_{acc}), which sets the ultimate limit of a cavity. The lower critical field H_{c1} defines the field at which it is energetically favorable for flux to be located inside the superconductor instead of being expelled by Meissner currents. The vortex penetration field (H_{vp}) can potentially exceed H_{c1} in case of a surface barrier with the ultimate limitation set by the superheating field H_{sh}. Nb is the preferred material for fabricating SRF cavities because it possesses the highest H_{c1} and critical temperature T_{c} among all elemental superconductors. For clean Nb, H_{c1} is about 170 mT [1] and $H_{\mathrm{sh}} = 240$ mT [2] at a temperature of 2 K corresponding to E_{acc} of about 40 and 55 MV m^{-1} for elliptical cavities. Some SRF cavities baked at 120 °C for 48 h in vacuum or low pressure gas atmosphere (i.e., LTB) have reached peak surface magnetic fields exceeding H_{c1} but for mass production operating E_{acc} values around 30 MV m^{-1}or below are chosen [3].

In the context of LTB study, it is important to understand the underlying mechanisms that can influence the material properties. The effect of LTB treatments can induce changes in the outermost nanoscale region of the material through diffusion processes. This results in the formation of a dirty layer with a larger London penetration depth (λ_{L}) compared to the bulk value of the material [4, 5]. This layer could potentially lead to a reduction of Meissner currents and the formation of a surface barrier at the interface between the outer dirty layer and the bulk material [6]. Consequently, this scenario can be viewed as the creation of a potential bilayer superconductor. In a bilayer superconductor when the top layer penetration depth is larger than the substrate's two effects occur. First, H_{vp} into the surface layer is increased due to strong suppression of Meissner current. Second, an interface energy barrier between the layers [6] similar to the Bean-Livingston barrier [7] at the vacuum-superconductor interface is created potentially prohibiting flux penetration into the substrate up to the substrate's H_{sh}.

μSR experiments have reported evidence for an interface barrier in bilayer samples of different materials and thicknesses [8] and a slight increase of H_{vp} above H_{c1} for LTB samples. Magnetometry measurements could not confirm the enhancement for LTB samples [9] and we, therefore, hypothesize that the $H_{\mathrm{vp},\mu}$ for LTB was due to increased accumulation of vortices caused by vortex pinning in the near-surface region. Pinning centers can act as supplementary barriers, impeding the movement of vortices from the edges of the sample to the center [8]. As a result, they introduce additional resistance which leads to a delayed flux propagation towards the center of the samples compared to a scenario without pinning. Note that the implantation depth in so-called surface μSR experiments using a ~4.1 MeV beam is on the order of 130 µm for Nb. The aim of this study is to test whether flux could have been trapped in a thin layer comparable to this length scale before being detected by muons. In this case one would find $H_{\mathrm{vp},\mu} > H_{\mathrm{vp}}$. Understanding the dominant mechanism at play is crucial for guiding further developments in materials and layered structures beyond conventional bulk Nb technology.

DESCRIPTION OF EXPERIMENT

Brief General Description of the Muon Spin Rotation Technique

μSR is a powerful condensed matter technique for the direct measurement of the magnetic field inside the sample. In this experiment, 100% spin-polarized radioactive muons (μ^+) were implanted into the sample one at a time

* asadm@uvic.ca
† junginger@uvic.ca

ISBN: 978-3-95450-234-9 ISSN: 2673-5504 doi:10.18429/JACoW-SRF2023-MOPMB005

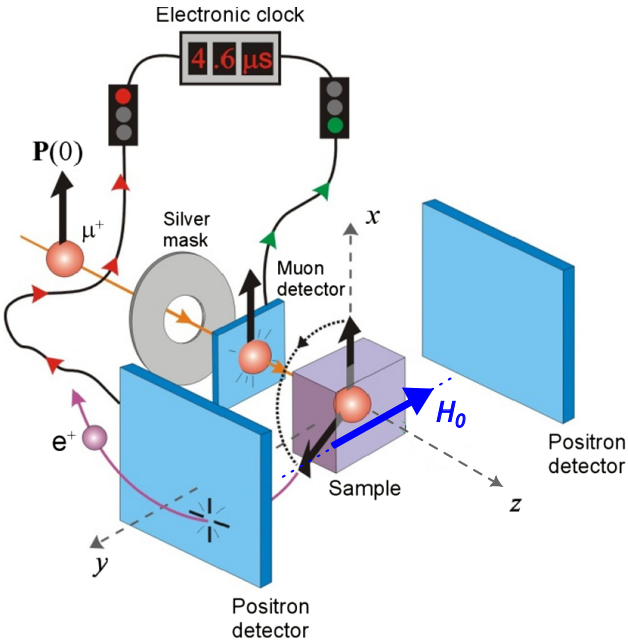

Figure 1: Principle of a μSR experiment in an externally applied transverse magnetic field H_0. Redrawn from Ref. [10]

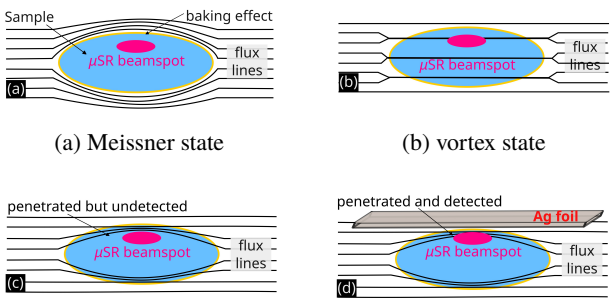

(a) Meissner state (b) vortex state

(c) vortex state with pinning (d) vortex state with pinning

Figure 2: Different superconducting states of Nb ellipsoidal samples with μSR beamspots: (a) Meissner state (pin-free sample), (b) vortex state (pin-free sample), (c) vortex state at early flux penetration due to the surface pinning when the flux penetration is undetected by the μSR beam spot, and (d) vortex state with pinning when flux penetration is detected by reducing the μ^+ implantation energy E using Ag foil.

at an energy of approximately 4.1 MeV in a transverse applied magnetic field arrangement (see Fig. 1). The muon spin precesses at the Larmor frequency, ω_μ which is proportional to the local magnetic field, B via gyromagnetic ratio of muon, γ_μ (i.e., $\omega_\mu = \gamma_\mu B$). Due to its very short lifetime ($\tau_\mu = 2.2\,\mu$sec), its decay positron preferentially in the same direction as the muon spin at the time of decay. The anisotropic distribution of the decay is measured using a set of positron detectors symmetrically placed around the sample. This allows for the temporal evolution of the muon's spin orientation to be deduced, and consequently, the properties of the magnetic fields it experiences.

Sample Geometry

We prepared ellipsoidal samples of LTB Nb and Nb_3Sn (2 µm)/Nb. Ellipsoidal samples were chosen due to their absence of edge boundaries, ensuring a uniform "geometric" magnetic response. Moreover, these samples are less prone to pinning due to their low demagnetizing factor of $N = 0.13$ [11]. In the ideal case of a pin-free sample, as shown in Fig. 2a, magnetic flux is completely expelled from the interior of the superconductor. The onset of magnetic flux penetration occurs at H_{vp} through vortex condensation as depicted in Fig. 2b, which are normal conducting cores of magnetic flux surrounded by supercurrents.

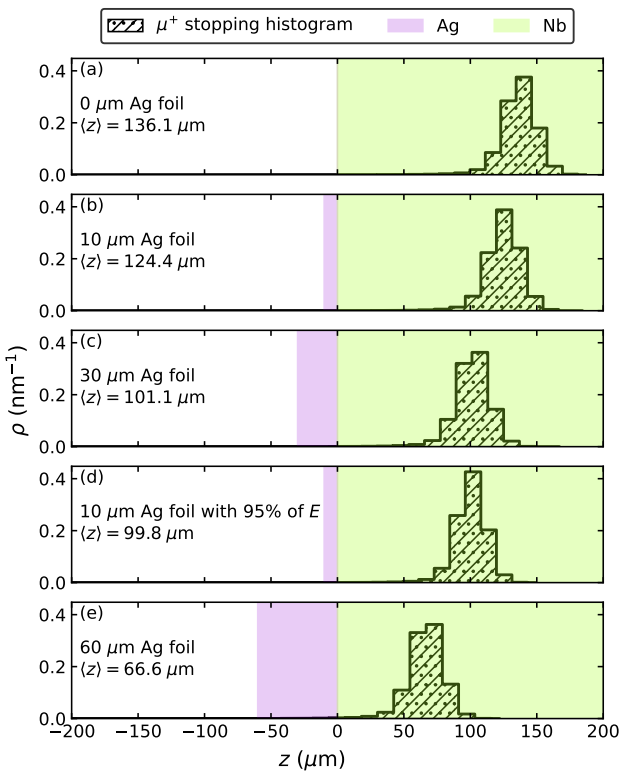

Figure 3: Simulated stopping profiles of "surface" muons in Nb with moderating Ag foil as a function of stopping depth, z. The light green color represents Nb material while the dark violet color represents the Ag foil of different thicknesses. The black hatches denote the μ^+ stopping histogram. The mean depth $\langle z \rangle$ of μ^+ corresponding to the thickness's of Ag foil is provided in the inset of each panel.

Concept of Experiment with Moderating Foils

As discussed in the Background section, in the μSR experiments trapped flux pinning could remain undetected (e.g., Fig. 2c) in the near surface region (i.e., <130 µm). To address this, in our experiment, we introduced layer(s) of Ag foil in front of the sample to reduce the implantation energy of μ^+ and consequently attenuate the stopping depth, as shown in Fig. 2d. If the enhancement in H_{vp} is caused by surface pinning, the flux will be detected at a lower field, resulting in a reduced value of $H_{vp,\mu}$. Alternatively, if it

ISBN: 978-3-95450-234-9 ISSN: 2673-5504 doi:10.18429/JACoW-SRF2023-MOPMB005

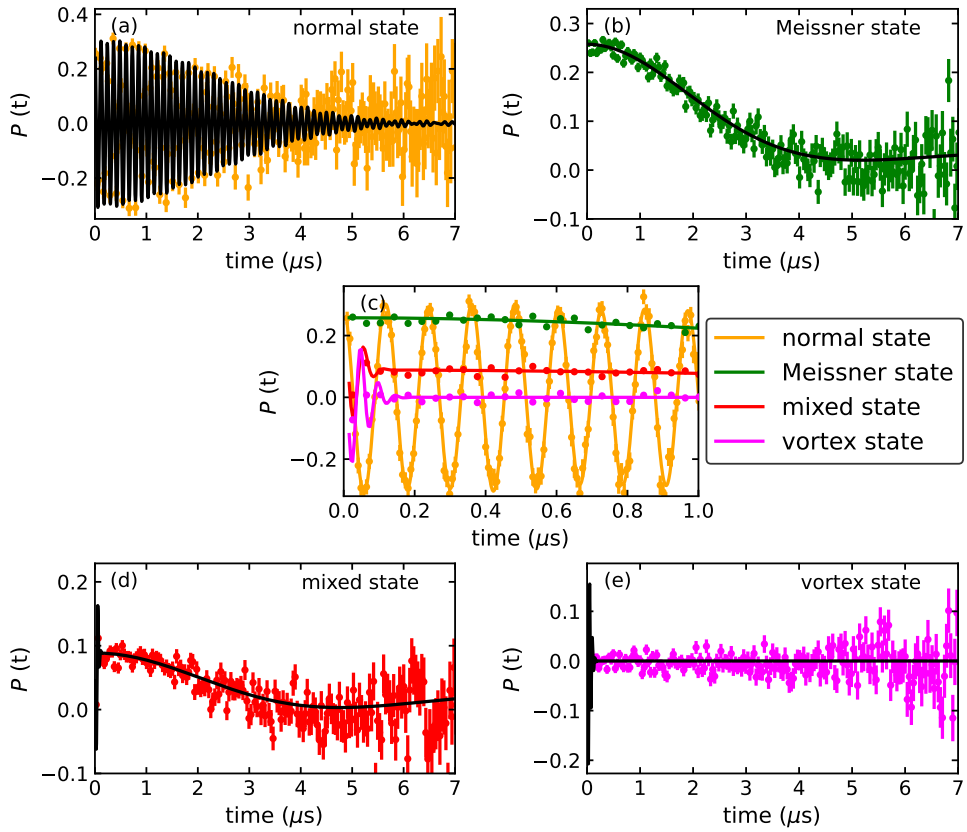

Figure 4: The depolarization of μ^+ with fit-functions in the LTB Nb (no foil) in (a) normal state, (b) Meissner state, (d) mixed state (Meissner + vortex state), and (e) vortex state. For comparison, all the states in a smaller timescale are plotted in (c). The colored closed circles with error bars represent the data points, and the solid lines represent the fits to the data using Eq. (1).

is due to an interface barrier, $H_{\mathrm{vp},\mu}$ will remain unchanged compared to the measurement without the foil.

Implantation Profile

The range of implanted "surface" muons in a Nb target on TRIUMF's M20 beamline, including a moderating Ag layer of variable thickness (indicated in Fig. 3's inset) were simulated using the Stopping and Range of Ions in Matter (SRIM) Monte Carlo code [12]. Each simulation involved 1×10^6 projectiles with a kinetic energy of approximately 4.1 MeV in Nb (density = 8.57 g cm^{-3}). To implant μ^+ at different stopping depths, z, we placed Ag foil layer(s) (density = 10.49 g cm^{-3}) in front of the Nb targets. The simulation results indicate that the thicker foil reduces the energy most, resulting in the shortest average implantation depth, $\langle z \rangle$ of μ^+ in Nb. Although we present the simulation results for Nb here, similar simulations were performed for Nb_3Sn (2 µm)/Nb samples as well.

RESULTS

Polarization Functions

The time differential asymmetry signal of μ^+ contains the local field information in the Nb sample. As a result, different superconducting states (i.e., different magnetic field distributions) can be observed in the sample as shown in Fig. 4 by varying the applied field H_0 from zero magnetic field to well above H_{c1}. Here, the frequency of oscillation and damping of the signal exhibit significant variations depending on the superconductor's different states. Consequently, the polarization signal contains information on the volume fraction of the host material sampled by the μ^+ that does not contain a magnetic field. Hence, this signal can be used to characterize the transition from Meissner to vortex state. The complete polarization function $P(t)$ is a sum of two terms:

$$P(t) = f_0 \cdot P_{\mathrm{ZF}}^{\mathrm{dyn}}(t) + f_1 \cdot P_{\mathrm{Gaussian}}(t), \qquad (1)$$

where f_0 is the initial asymmetry related to the dynamic Kubo-Toyabe function, $P_{\mathrm{ZF}}^{\mathrm{dyn}}(t)$ corresponding to an absence of a local magnetic field, and f_1 is the amplitude related to a weakly damped oscillating function $P_{\mathrm{Gaussian}}(t)$ corresponding to the measurement of the existence of local field distribution. Here,

$$P_{\mathrm{ZF}}^{\mathrm{dyn}}(t) = P_{\mathrm{ZF}}^{\mathrm{stat}}(t)\exp(\nu t) + \nu \int_0^t dt' \left\{ P(t-t') P_{\mathrm{ZF}}^{\mathrm{stat}}(t') \exp(-\nu t') \right\}, \qquad (2)$$

ISBN: 978-3-95450-234-9 ISSN: 2673-5504 doi:10.18429/JACoW-SRF2023-MOPMB005

here

$$P_{\mathrm{ZF}}^{\mathrm{stat}}(t) = \frac{1}{3} + \frac{2}{3}\left[1 - (\sigma_0 t)^2\right]\exp\left[-\frac{1}{2}(\sigma_0 t)^2\right], \quad (3)$$

and

$$P_{\mathrm{Gaussian}}(t) = \exp\left(-\frac{1}{2}\sigma_1^2 t^2\right)\cdot\cos\left(\omega t + \frac{\pi\phi}{180}\right), \quad (4)$$

where σ_i = damping rate, ν = hopping rate, and ϕ = phase factor. The more details of the fit functions can be found elsewhere [8].

Figure 4 illustrates the asymmetry as a function of time in the LTB Nb (no foil). It showcases different scenarios: (a) In the normal state all muons probe almost the same field yielding weaker damping fitted by $P_{\mathrm{Gaussian}}(t)$. (b) In the Meissner state the depolarization is caused by randomly orientated nuclear dipole fields resulting in the characteristic $P_{\mathrm{ZF}}^{\mathrm{dyn}}(t)$ function. (c) In the mixed state, which is defined by coexisting macroscopic areas in the Meissner and vortex state, combines the $P_{\mathrm{ZF}}^{\mathrm{dyn}}(t)$ polarization function with a rapidly decaying $P_{\mathrm{Gaussian}}(t)$ function. (d) In the vortex state, all muons sense the external field and there is no signature of the $P_{\mathrm{ZF}}^{\mathrm{dyn}}(t)$ polarization function left. Our interest is to observe the initial asymmetry f_0 corresponding to the Meissner state, enabling us to investigate the $H_{\mathrm{vp},\mu}$ while varying the implantation depth of μ^+.

Fit Parameter f_0 as a Function of Applied Field H_0

In Fig. 5, the fit parameter f_0 of Eq. (1) at different $\langle z\rangle$ were plotted against the (effective) applied magnetic field H_0. Note that, to account for the field enhancement of our sample, we used the demagnetization factor $N = 0.13$ as described in [11]:

$$H_0 = H_{\mathrm{applied}} \times \frac{1}{1-N}, \quad (5)$$

here, H_{applied} is the applied field calibrated to the normal state (i.e., above T_c) field measurements of the same sample.

f_0 signifying the volume fraction probed by the muons which is in the field free Meissner state. Since this state is characterized by the absence of any magnetic field within the sample, resulting in the maximum value of f_0. As the system transitions to the mixed state, which consists of coexisting regions of Meissner and vortex states, the total signal is shared between f_0 and f_1. With further increase in the field strength, f_0 eventually reaches zero, indicating that the entire probed area by the muons has transitioned into the vortex state.

To compare the $H_{\mathrm{vp},\mu}$ values at different $\langle z\rangle$ of μ^+, we employed a phenomenological fit function:

$$f_0(H_0) = \frac{L}{1+\exp(-k(x-H_{\mathrm{mid}}))}, \quad (6)$$

where L represents the height of the curve, k is the steepness of the curve, and H_{mid} denotes the field at $f_0(H_0) = 0.5$. We define $H_{\mathrm{vp},\mu}$ as the applied field strength at which $f_0(H_0) = 0.95$ (shown by gray dotted lines in Fig. 5).

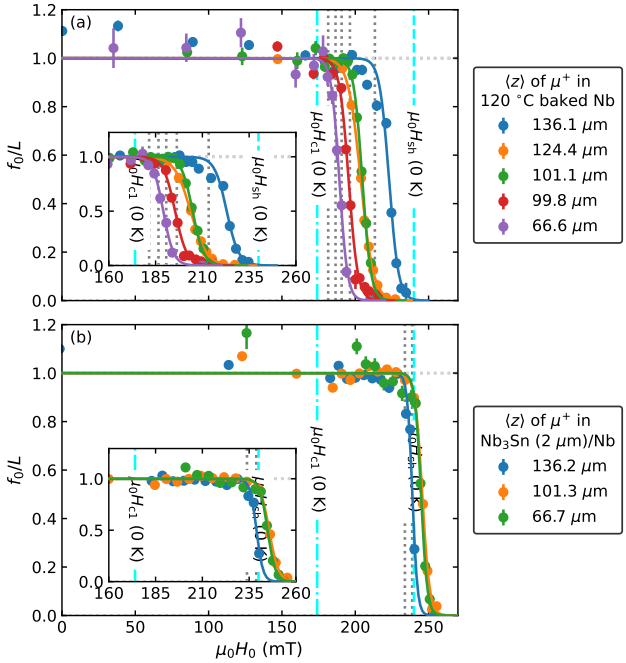

Figure 5: f_0 as a function of H_0 (a) in 120 °C baked (i.e., LTB) Nb and (b) in Nb_3Sn (2 μm)/Nb, at different $\langle z\rangle$ of μ^+ (shown in the inset). Colored closed circles represent the data points, and solid lines represent the fits to a phenomenological function given by Eq. (6). The gray color dotted curves indicate $H_{\mathrm{vp},\mu}$ for different $\langle z\rangle$. The cyan color dash-dot and dashed lines are corresponding values of H_{c1} and H_{sh} at $T = 0$ K. The small inset figures provide a zoomed scale of the same data near H_{vp}.

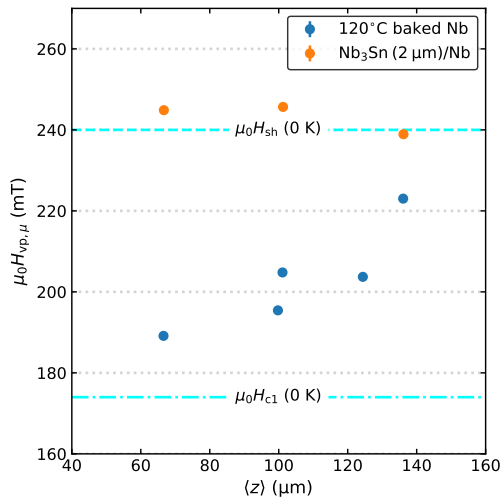

Figure 6: The $H_{\mathrm{vp},\mu}$ of both the samples are plotted as a function of $\langle z\rangle$ of μ^+. The blue and orange closed circles correspond to the data for 120 °C baked (i.e., LTB) Nb and Nb_3Sn (2 μm)/Nb. The cyan color dash-dot and dashed lines are corresponding values of H_{c1} and H_{sh} of Nb at $T = 0$ K.

ISBN: 978-3-95450-234-9 ISSN: 2673-5504 doi:10.18429/JACoW-SRF2023-MOPMB005

Now, in order to compare the values of $H_{\mathrm{vp},\mu}$ in both samples with the quantities $H_{\mathrm{c1}}(0\,\mathrm{K})$ and $H_{\mathrm{sh}}(0\,\mathrm{K})$ (represented by the cyan color dashed and dash-dot lines in Fig. 5) of Nb, a scaling factor has been applied to $H_{\mathrm{vp},\mu}$ using an empirical relation expressed by:

$$H(T) = H(0\,\mathrm{K})\left(1 - \left(\frac{T}{T_{\mathrm{c}}}\right)^2\right), \tag{7}$$

where T = measurement's temperature (i.e., $\leq$2.8 K) and T_{c} is the assumed critical temperature of 9.25 K [1]. The literature value of $\mu_0 H_{\mathrm{c1}}(0\,\mathrm{K}) = 174\,\mathrm{mT}$ [1], $\mu_0 H_{\mathrm{sh}}(0\,\mathrm{K}) = 240\,\mathrm{mT}$ [2] are used for Nb. In Fig. 6, we present the corresponding $H_{\mathrm{vp},\mu}$ values for both samples.

The analysis of the data presented in Fig. 6 reveals interesting observations regarding the behavior of $H_{\mathrm{vp},\mu}$ at varying $\langle z \rangle$. As the μ^+ implanted at shallower depths closer to the surface, a noticeable decrease in the $H_{\mathrm{vp},\mu}$ value is observed. This decrease aligns with the previously observed surface pinning effect in the 120 °C baked Nb sample, providing further consistency to the phenomenon. In contrast, when considering the Nb_3Sn (2 µm)/Nb sample, the $H_{\mathrm{vp},\mu}$ value remains constant across different depths. This behavior can be attributed to the presence of an interface barrier within the sample structure.

CONCLUSION

The main conclusions which can be drawn from this study are:

- The results suggest that the $H_{\mathrm{vp},\mu}$ is enhanced by surface pinning in the low temperature baking Nb.
- Alternatively, $H_{\mathrm{vp},\mu}$ remains unchanged at different depths in the bilayer Nb_3Sn (2 µm)/Nb superconductor due to the interface barrier.
- Finally, we confirm that an overlayer on Nb can push the first field of vortex penetration close to the superheating field.

ACKNOWLEDGEMENTS

We acknowledge the support of the Natural Sciences and Engineering Research Council of Canada (NSERC), SAPPJ-2020-00030 and SAPIN-2021-00032. The authors would like to thank Bhalwinder Waraich for fabrication of the ellipsoid and flat coin samples and Daniel Leslie Hall for providing the Nb_3Sn treatments. Thanks to Gerald Morris, Bassam Hitti, Donald Arseneau, Deepak Vyas, Rahim Abasalti, and Iain McKenzie from the TRIUMF CMMS support team.

REFERENCES

[1] D. K. Finnemore, T. F. Stromberg, and C. A. Swenson, "Superconducting properties of high-purity niobium," *Phys. Rev.*, vol. 149, pp. 231–243, 1966. doi:10.1103/PhysRev.149.231

[2] M. K. Transtrum, G. Catelani, and J. P. Sethna, "Superheating field of superconductors within Ginzburg-Landau theory," *Phys. Rev. B*, vol. 83, p. 094 505, 2011. doi:10.1103/PhysRevB.83.094505

[3] H. Padamsee, "History of gradient advances in SRF," 2020. doi:10.48550/arXiv.2004.06720

[4] A. Romanenko, A. Grassellino, F. Barkov, A. Suter, Z. Salman, and T. Prokscha, "Strong meissner screening change in superconducting radio frequency cavities due to mild baking," *Appl. Phys. Lett.*, vol. 104, p. 072 601, 2014. doi:10.1063/1.4866013

[5] R. M. L. McFadden, M. Asaduzzaman, T. Prokscha, Z. Salman, A. Suter, and T. Junginger, "Depth-resolved measurements of the meissner screening profile in surface-treated Nb," *Phys. Rev. Appl.*, vol. 19, p. 044 018, 2023. doi:10.1103/PhysRevApplied.19.044018

[6] T. Kubo, "Multilayer coating for higher accelerating fields in superconducting radio-frequency cavities: A review of theoretical aspects," *Supercond. Sci. Technol.*, vol. 30, p. 023 001, 2017. doi:10.1088/1361-6668/30/2/023001

[7] C. P. Bean and J. D. Livingston, "Surface barrier in type-ii superconductors," *Phys. Rev. Lett.*, vol. 12, pp. 14–16, 1964. doi:10.1103/PhysRevLett.12.14

[8] T. Junginger, W. Wasserman, and R. E. Laxdal, "Superheating in coated niobium," *Supercond. Sci. Technol.*, vol. 30, p. 125 012, 2017. doi:10.1088/1361-6668/aa8e3a

[9] D. A. Turner, G. Burt, and T. Junginger, "No interface energy barrier and increased surface pinning in low temperature baked niobium," *Sci. Rep.*, vol. 12, p. 5522, 2022. doi:10.1038/s41598-022-09023-0

[10] A. Grassellino *et al.*, "Muon spin rotation studies of niobium for superconducting rf applications," *Phys. Rev. Spec. Top. Accel. Beams*, vol. 16, p. 062 002, 2013. doi:10.1103/PhysRevSTAB.16.062002

[11] T. Junginger *et al.*, "Field of first magnetic flux entry and pinning strength of superconductors for rf application measured with muon spin rotation," *Phys. Rev. Accel. Beams*, vol. 21, p. 032 002, 2018. doi:10.1103/PhysRevAccelBeams.21.032002

[12] J. F. Ziegler, M. Ziegler, and J. Biersack, "SRIM – The stopping and range of ions in matter (2010)," *Nucl. Instrum. Methods Phys. Res., Sect. B*, vol. 268, pp. 1818–1823, 2010. doi:10.1016/j.nimb.2010.02.091